Mechanics Research Communications 43 (2012) 57–65

Contents lists available at SciVerse ScienceDirect

Mechanics Research Communications

journal homepage: www.elsevier.com/locate/mechrescom

Experimental measurements and numerical modeling of dynamic compression response of an interpenetrating phase composite foam

C. Periasamy, H.V. Tippur*

Department of Mechanical Engineering, Auburn University, Auburn, AL 36849, United States

ARTICLE INFO

Article history:
Received 2 August 2011
Received in revised form 23 January 2012
Available online 16 March 2012

Keywords:
Structural foams
Syntactic foams
Hybrid materials
High strain rate measurements
Compression
Finite element analysis
Infinite elements

ABSTRACT

A 3D interpenetrating phase composite (IPC) foam made by infusing syntactic foam (SF) into an open-cell aluminum scaffold is studied under high-strain rate conditions. The SF is prepared by dispersing hollow glass microballoons into an epoxy matrix. Dynamic compression characteristics, including strength and failure progression of pure SF and IPC foam made of four different volume fractions of microballoons in SF measured using a split Hopkinson pressure bar (SHPB) apparatus are reported. The results show that in general IPC foams outperform SF in terms of compressive strength. An idealized 3D elasto-plastic unit-cell based finite element (FE) model is proposed for studying the IPC foam. The 3D geometry of the aluminum constituent in the cubic unit-cell is modeled as a tetrakaidecahedron, whereas the SF constituent is modeled as the occupant of the rest of the unit-cell. The computational model incorporates infinite elements to represent the far-field regions surrounding the unit-cell. Comparisons of computational and experimental results for different microballoon volume fractions of SF are reported.

1. Introduction

Recent advances in commercial and defense automotives, as well as aerospace and marine construction, require innovative lightweight materials that are stiff and tough structures capable of absorbing impact energy. This concurrence of material properties cannot be formulated into a single material system easily. Interestingly, some naturally occurring materials such as bone and nacre exhibit this feature. Such materials have a 3D interpenetrating microstructure, often made up of two or more biological phases resulting in the enhancement of the overall structural properties. Artificial multi-phase composites having a 3D interpenetrating structure are often referred to as interpenetrating phase composites (IPC) (Clarke, 1992). In general, IPCs are composite materials in which each constituent forms a continuous 3D network within the material volume. Thus, each phase in its standalone state can be imagined to have an open-cellular microstructure. Even though IPCs are heterogeneous on a micro/meso scale, the macro scale response is often isotropic. Each phase offers its own unique property to the IPC as a whole. For example, one phase might offer good toughness and thermal conductivity, while the other might enhance stiffness and dielectric properties. That is, each phase of an IPC contributes its unique property to the overall structural response synergistically. This co-existence of desirable properties without significant directional dependency or distinct weak planes (as opposed to conventional layered composites) make IPC attractive for structural applications.

Material processing details and experimental measurements on one such IPC made of two phases – syntactic foam (SF) and aluminum foam has been presented by the authors under static and dynamic loading conditions in an earlier paper (Periasamy et al., 2010). In the current work, the dynamic compression responses of SF and IPC foam along with finite element modeling of IPC foam are presented. The finite element model is based on a unit-cell approach. That is, a repeating cubic volume element of IPC foam consisting of a single aluminum open-cell and a SF region penetrating the aluminum scaffold within the cubic volume. The geometric and finite element modeling aspects of the unit-cell IPC are discussed in this paper. Infinite elements are used in the model to discretize the far field regions surrounding the unit-cell. A brief background on these infinite elements, the implementation issues and calibration work are also presented for completeness. Subsequently, results from finite element analysis of IPC foam and their comparison with experimental are presented.

2. Experimental details

2.1. Sample preparation

The constituents used for preparing SF were a low viscosity epoxy (Epo-Thin™ from Beuhler, Inc. USA, mass density of the resin ~1100 kg/m^3) and hollow glass microballoons (K1™

* Corresponding author. Tel.: +1 334 844 3327.
E-mail addresses: tippuhv@auburn.edu, htippur@eng.auburn.edu (H.V. Tippur).

0093-6413/$ – see front matter © 2012 Elsevier Ltd. All rights reserved.
doi:10.1016/j.mechrescom.2012.03.002

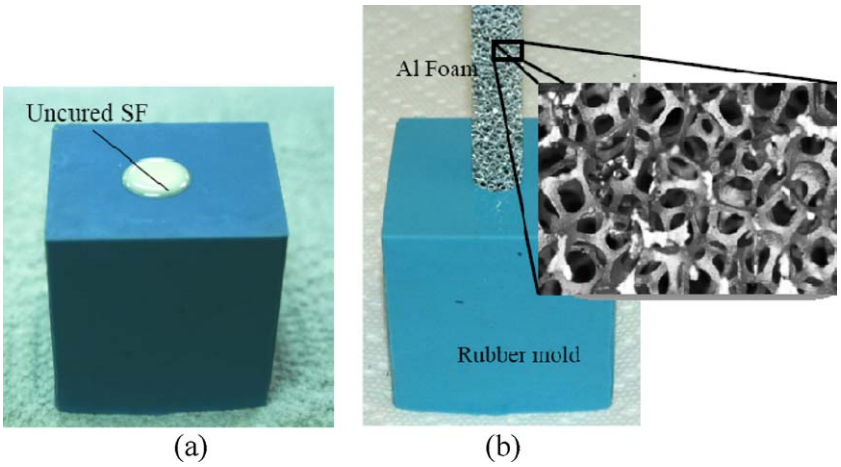

Fig. 1. Sample preparation for syntactic foam (SF) and interpenetrating phase composite (IPC) foams (a) rubber mold with uncured SF, (b) aluminum mold inserted into mold containing uncured SF.

microballoons from 3 M Corp., bulk density 125 kg/m^3) of average diameter ~60 μm and wall thickness ~0.6 μm. SF samples were prepared by mixing the desired quantity of microballoons into epoxy resin. The uncured syntactic foam was vacuumed (at approximately −75 kPa gage pressure) to remove any trapped air bubbles, then transferred into a silicone rubber mold (Fig. 1). The mixture was then allowed to cure in the mold for at least seven days before being removed and machined to size as shown in Fig. 2.

The metal foam used in the IPC was an open-cell Duocel® aluminum (Al 6101-T6) preform (ERG Aerospace Corp., USA) with a pore density of 40 pores per inch (~8% relative density). The metal foam was degreased with acetone and then coated with silane, γ-aminopropyltrimethoxysilane ($H_2NC_2H_4NHC_3H_6Si(OCH_3)_3$), to enhance wetting and hence the bond strength between aluminum ligaments and syntactic foam. To prepare the IPC foam, the degassed, uncured SF was prepared as described earlier. Then, the silane coated aluminum foam was slowly lowered into the mold (as shown in Fig. 1(b)) containing uncured syntactic foam so that the syntactic foam filled the open-pores of the aluminum network. Although gelling of SF occurs within a few hours, the cast was allowed to slowly cure for at least seven days. The cured cast was then removed from the mold and cut into small cylindrical samples (Fig. 2) whose flat ends were finished using a milling machine.

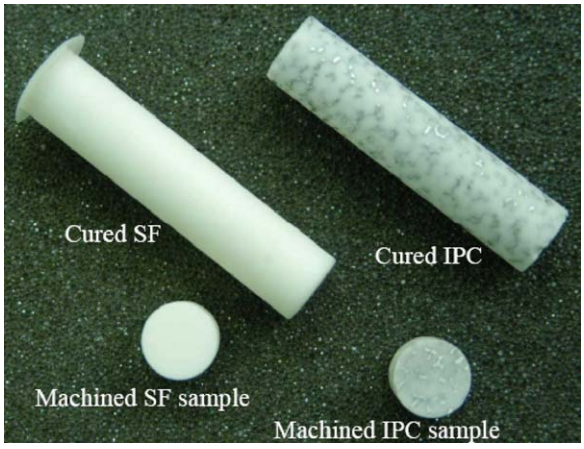

Fig. 2. As cast and machined SF and IPC foam samples.

2.2. Sample dimensions

The sample dimensions were determined based on a previous work by Gibson (2000). Gibson has analyzed the cell size effects in open-cell foams and proposed a specimen thickness (length) to cell size ratio (t/d) of 8 or above, so that the specimen represents the bulk. By size effects, Gibson means the effect of cell size on the measured material properties when the macroscopic sample dimensions are of the order of the cell size. The aluminum foam used in this work has a pore density of 40 pores per inch with 22–26 cells per inch. Therefore, it can be assumed that there are approximately 24 cells per inch on an average (Fig. 3(a) shows the relative sizes of pores and cells). Thus, the individual cell size is approximately 1.06 mm (0.042 in.). A t/d ratio of 9 was chosen for the SHPB tests. Accordingly, the samples used in the dynamic testing were machined to have a length of 9.5 mm (0.375 in.) and a diameter of 12.7 mm (0.5 in.) as shown in Fig. 3(b).

From the dimensions shown in Fig. 3(b), the thickness (t) to diameter (D) ratio (or, slenderness ratio S_0) is 0.75. This S_0 was chosen with reference to the work published by Malinowski and Klepaczko (1986) in which they suggest an optimum S_0 for use in SHPB tests for different material categories based on the axial inertia and interfacial friction of the sample material. According to their work, samples made of low flow stress materials (gold and uranium) should have $0.1 \leq S_0 \leq 0.5$. For samples made of moderate density metals such as aluminum and copper they suggest an optimum S_0 range of 0.5–1.0 and for hard materials (high strength steels), an optimum S_0 range of 1.0–1.5. The IPC foam used in this work consists of aluminum and SF, which are made of moderately dense and brittle, but not hard materials. The combined effect the two materials suggests a S_0 in the 0.5–1.0 range for the SHPB test samples. Four different types of SF and IPC foam samples were prepared by using different volume fractions (V_f = 10%, 20%, 30% and 40%) of microballoons in epoxy. Accordingly, the different samples were labeled in a self explanatory fashion as SF-10, SF-20, SF-30, SF-40, IPC-10, IPC-20, IPC-30 and IPC-40.

3. Experimental results

SF and IPC foam samples with 10%, 20%, 30% and 40% microballoon volume fractions were tested at a strain rate of ~1500 per second using a split Hopkinson pressure bar apparatus. At least four specimens were tested for each volume fraction. Details on calibration, strain rate measurement and stress equilibrium issues

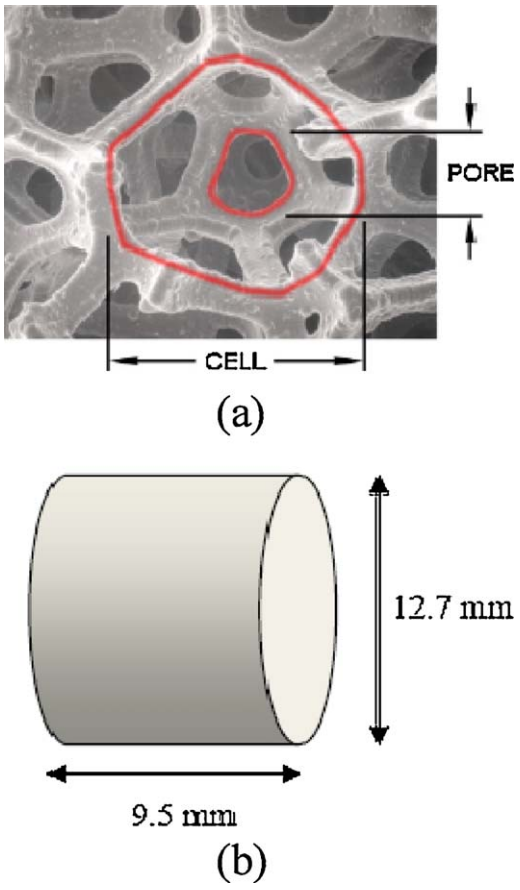

Fig. 3. (a) Representation of pores and cells in open-cell aluminum foam scaffold, (b) sample dimensions used for split-Hopkinson pressure bar tests.

about the SHPB experiments have been previously presented by Periasamy et al. (2010). The maximum strain attained by a sample depends on the time period of the incident stress wave. This in turn depends on the length of the striker used (Meyers, 1994). Several striker lengths, 203 mm (8 in.)–406 mm (16 in.), were considered in this work. In view of a relatively large strain expected for the sample to fail, the longest feasible striker length was considered. The incident stress pulse generated by the 406 mm long striker (impact velocity ~15 m/s) had a total time period of ~200 μs with constant strain lasting over 100 μs (Fig. 4). The maximum true strain

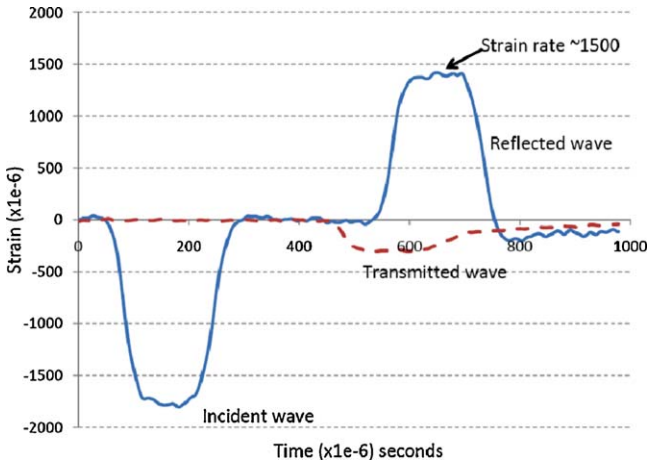

Fig. 4. Typical strain histories for SF-30 material obtained from the SHPB bars using a 406 mm aluminum striker.

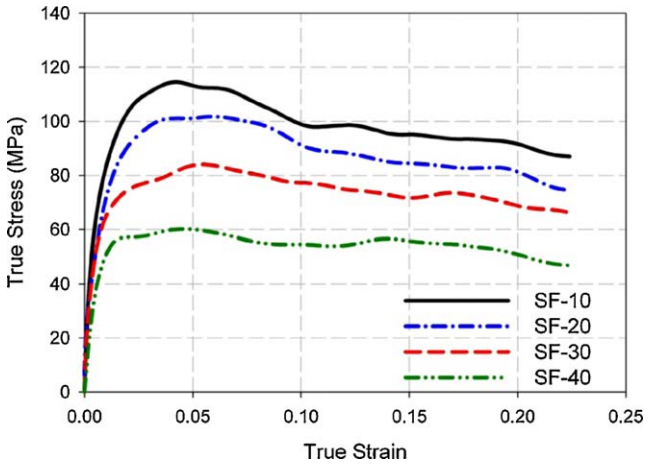

Fig. 5. Effect of microballoon volume fraction on dynamic stress–strain response of SF samples (strain rate ~ 1500 s^{-1}).

experienced by the sample for this pulse was a little over 22%. So, conservatively, all analyses were based on a maximum specimen true strain value of 22% and the stress–strain data once the stress pulse started dropping off was not considered in the analyses.

3.1. Syntactic foam response

The dynamic true stress–true strain responses of SF with four different volume fractions of microballoons obtained using a 406 mm striker at a strain rate of ~1500 per second are shown in Fig. 5. The measured response of syntactic foam has two distinct regions. An initial elastic response is followed by a monotonically decreasing stress region with increasing strain. The compressive strengths of the samples decrease with increasing microballoon volume fraction. The compressive strengths[1] of the 10%, 20%, 30% and 40% volume fraction samples were approximately 104 ± 4 MPa, 80 ± 3 MPa, 62 ± 5 MPa and 50 ± 3 MPa, respectively. The relative drop in the compressive strengths for every 10% increase in the microballoon volume fraction is ~20%. After yielding, the stresses for SF with lower V_f of microballoons remain consistently higher than that for SF with higher V_f. The difference between the post-yield stress values in samples with different volume fractions is approximately constant at all strains (within the observation window).

3.2. IPC foam response

The IPC samples of four microballoon volume fractions *viz*. 10% (IPC-10), 20% (IPC-20), 30% (IPC-30) and 40% (IPC-40) were tested and the results are shown in Fig. 6. The dynamic compression response of IPC foams followed trends similar to that of the corresponding syntactic foams. The response shows a linear region in the beginning, followed by a modest nonlinear response until a maximum stress is reached. Subsequently a monotonic reduction of stress with increasing strain is seen in the observation window up to ~22% true strain. As in the case of SF samples, the yield strengths of IPC foam samples decrease with increasing volume fraction of microballoons. In the order of increasing microballoon V_f, the compressive strengths are approximately 120 ± 4 MPa, 100 ± 5 MPa, 79 ± 6 MPa and 58 ± 3 MPa. The percentage decrease in the compressive strength for the IPC-20 with respect to that of IPC-10 is 16%, and that of IPC-30 with respect to that of IPC-20 is 21%. The

[1] The yield stress was estimated to be the value between the start of non-linearity and the peak value.

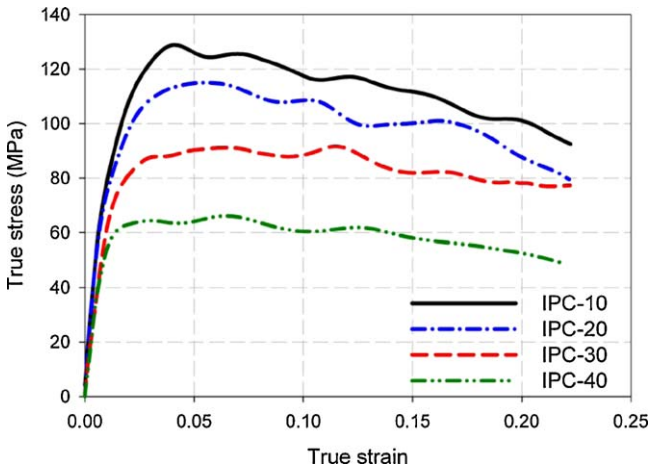

Fig. 6. Effect of microballoon volume fraction on dynamic stress–strain response of IPC foam samples (strain rate ~ 1500 s^{-1}).

IPC-40 has a 26% reduction in compressive strength with respect to IPC-30.

In both SF and IPC, the observed decrease in strength with increasing microballoon volume fraction is attributed to the increased void volume fraction within the SF. This results in a favorable condition for more number of internal cracks to originate from the voids. This in turn leads to lower strength at higher microballoon volume fraction in SF. Detailed measurements and micrographic analysis of failed SF and IPC have been documented in an earlier work (Periasamy et al., 2010).

4. Finite element modeling

The enhanced dynamic compression response of IPC foam samples and its complex 3D geometry were motivations to analyze it using finite element method. For this purpose, a 3D model of IPC foam with SF and aluminum domains had to be developed. In the actual IPC foam, the aluminum cells are randomly shaped and oriented in the 3D space. Numerical simulation of a full scale 3D representation of IPC foam using nonlinear transient analysis will require tremendous computational effort. Therefore, an idealized unit-cell model of the IPC foam was used for the geometric model which considerably reduced the computational requirements.

4.1. Geometric modeling

In a previous study on the compressive response of unfilled open-cell foams, Gong et al. (2005) have reported that the number of sides of a cell range from 9 to 17, the average being 14 (see, insert in Fig. 1(b)). Accordingly, they chose a 14 sided polyhedron (tetrakaidecahedron) (Thomson, 2008) called a Kelvin cell to idealize a single cell of the open-cell foam. In the current work, the same Kelvin cell geometry was adopted for the unit-cell model of the aluminum open-cell foam. The polyhedron consists of six squares and eight hexagons, with all the edges/ligaments having the same length l, as shown in Fig. 7. Duocel® foam is known to show modest anisotropy in the rise and transverse directions (Gong et al., 2005). In this work, the aluminum cells are filled with SF that dominates the overall response of the IPC foam and hence geometric and mechanical anisotropy is not considered for simplicity of analysis. The height, h of the Kelvin cell is $h = 2\sqrt{2}l$. The unit-cell thus modeled could be viewed as a repeating volume element in 3D space as depicted by the 3D array of cells shown in Fig. 7.

The 3D geometry of the unit-cell IPC foam was constructed using Solid Edge™. The length and cross section of the aluminum ligaments in the model foam were proportionately chosen so that the volume fraction of aluminum in the model matches the volume fraction (8% as reported by the manufacturer) of aluminum in the actual test sample. The ligament cross section was approximated as an equilateral triangle. In reality however, the cross sections along the actual ligaments are thinner at the mid-span and thicker at the vertices of the polyhedron. Considering the complexity of modeling of such geometry, the ligaments were idealized as having a constant cross sectional dimension. The region not occupied by aluminum was discretized and "filled" with the SF material. Thus, the overall shape of the final unit-cell IPC foam model is a hexahedron.

Table 1
Elastic properties of SF (from SHPB measurements) and Al 6101 (from Alcoa Inc. datasheet) used in the finite element model.

Material	Elastic modulus (MPa)	Poisson ratio	Density (kg/m^3)
Aluminum 6101	69,600 ± 700	0.35	2700 ± 15
SF-10	5122 ± 160	0.34	995 ± 6
SF-20	4529 ± 95	0.34	870 ± 4
SF-30	4459 ± 140	0.34	796 ± 5
SF-40	3835 ± 115	0.34	696 ± 4

4.2. Material properties

The geometric model was imported into ABAQUS for finite element analysis. The dynamic compressive stress–strain response of SF measured using the SHPB was used as the material property input for the SF region of the model in the finite element analysis. The elastic modulus, Poisson's ratio and mass density of the different volume fraction SF that were used in the finite element analysis are shown in Table 1. The aluminum ligaments were assigned a bilinear stress–strain property corresponding to Al 6101 based on Alcoa Inc. datasheet. The properties of aluminum used in the analysis are shown in Tables 1 and 2.

Assumptions for the plastic material behavior of aluminum and SF include homogeneous, rate independent plastic strain, isotropic hardening and yielding based on von-Mises stresses. The flow rule

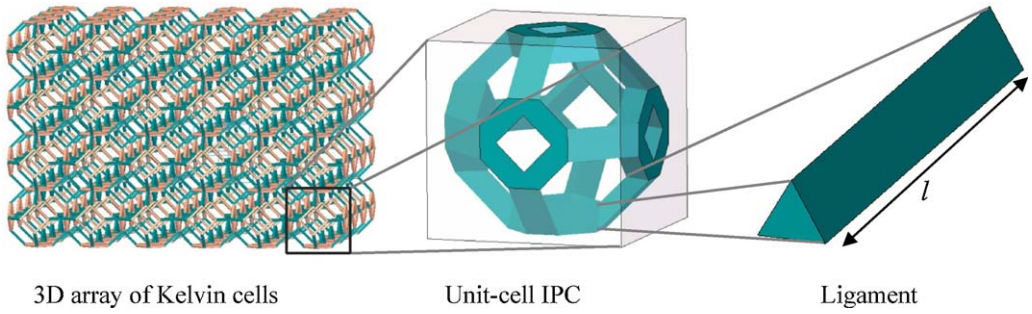

Fig. 7. Schematics representing the building blocks of an idealized Kelvin cell based IPC foam.

Table 2
Inelastic properties of Al 6101 (from Alcoa Inc. datasheet) used in the finite element model.

Plastic strain	Plastic stress (MPa)
0	172
0.148	200

associated with the von-Mises yield criterion is (Mendelson, 1983),

$$d\varepsilon_{ij}^{P} = \frac{3}{2}\frac{S_{ij}}{\sigma_e}d\varepsilon_p,$$

where ε_{ij}^{P} and ε_p are the plastic strain components and effective plastic strain, respectively, and S_{ij} and σ_e are the deviatoric stress components and effective stress, respectively.

4.3. Computational details

In order to model the dynamic behavior of the IPC foam, a 3D transient elasto-plastic analysis is necessary. However, due to the complexity of the geometry and the size of the resulting discretized model, an achievable goal of simulating a unit-cell situated deep in the bulk is attempted instead of a full-scale model. By doing this, certain approximations occur implicitly. The unit-cell model by itself has exposed faces, and does not represent a cell within the material volume. This is because in a dynamically loaded sample most of the stress waves travel through the entire length of the sample before partly reflecting at the sample boundaries. In reality, there will be transmission and reflection of stress waves at every material discontinuity/interface (between SF and aluminum). Considering this, a better model to analyze would be the one that has an array of unit-cells which repeat periodically in a 3D space. In other words, the number and arrangement of cells would be closer to the actual test sample. This however, demands very high computational resources. Therefore, the analysis in this work is restricted to a unit-cell model and the criteria for verifying the results from the FE model against the experimental results is restricted to only the measured stress–strain response. To prevent the stress waves from reflecting at the unit-cell boundaries, infinite elements (Bettess, 1977) were used. A layer of infinite elements that functionally simulate a large material volume encapsulating the unit-cell was modeled. In other words, the layer represents the far field surrounding the unit-cell. In doing so, the details of the intercellular transients are muted, yet the overall stress–strain response of the cell can be captured.

The 3D unit-cell IPC model was discretized using four node linear tetrahedrons. To check for the appropriateness of the mesh refinement, models meshed with elements having different edge lengths were studied for convergence. Based on the outcome, a model meshed with elements having an approximate element length of $(2/15)l$ where l is the ligament length, was selected.

4.3.1. Infinite elements

The infinite elements are used in situations where the region of interest is very small compared to the region surrounding it. One of the earliest and important work on infinite elements was carried out by Bettess (1977). Since its introduction, infinite elements have been developed and used by several researchers. For example, Haggblad and Nordgren (1987) used infinite elements to model the far field regions to study a nonlinear soil-structure interaction effect. Viladkar et al. (1991) also used infinite elements coupled with finite elements to idealize and study interactions between the far field soil regions and frame structures. Two types of infinite elements were developed and used by Park et al. (1991) to analyze the hydrodynamic forces on offshore structures. One type was used to model radiation in the fluid at infinity and the other type used to model the fictitious bottom boundary of a deep body of water. Later, Zhao and Valliappan (1993) developed a 3D dynamic infinite element. A detailed description of one type of dynamic 3D infinite element formulation can be found in a recent monograph by Zhao (2009).

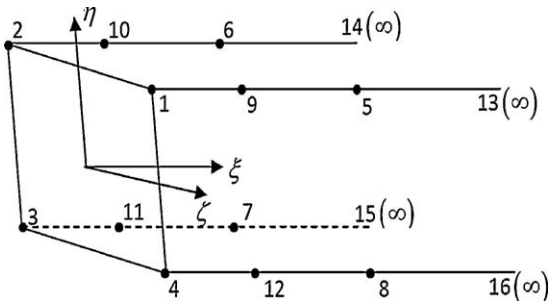

Fig. 8. Schematic of 3D infinite element used in dynamic compression simulations.

The relevant aspects of the element formulation are as follows in reference to a schematic of the 3D infinite element provided in Fig. 8. The derivation of the 3D dynamic infinite element is based on harmonic wave loading and hysteretic damping of the same. Arbitrary waves can be achieved by superposing several harmonic waves. The general governing equation of the 3D dynamic infinite element is,

$$-\omega^2[M]\{\Delta\} + (1 + i\eta_d)[K]\{\Delta\} = \{F_0\}, \tag{1}$$

where ω is the circular frequency of a harmonic wave, $[M]$ and $[K]$ are the global mass and stiffness matrices respectively, $\{\Delta\}$ is the unknown nodal displacement vector and $\{F_0\}$ is the amplitude vector of the applied harmonic load. The difference between an ordinary 3D dynamic finite element and a 3D dynamic infinite element is in their shape function matrix, $[N]$. For the infinite element, it is given by,

$$\begin{aligned}
N_q &= P_q(\xi)\left[\frac{1}{4}(1+\eta)(1+\zeta)\right] \quad (q = 1, 5, 9),\\
N_q &= P_q(\xi)\left[\frac{1}{4}(1+\eta)(1-\zeta)\right] \quad (q = 2, 6, 10),\\
N_q &= P_q(\xi)\left[\frac{1}{4}(1-\eta)(1-\zeta)\right] \quad (q = 3, 7, 11),\\
N_q &= P_q(\xi)\left[\frac{1}{4}(1-\eta)(1+\zeta)\right] \quad (q = 4, 8, 12),
\end{aligned} \tag{2}$$

where $P_q(\xi)$ is the wave propagation function, $q = 1, 2, \ldots, 12$ represents the 12 nodes of the infinite element in Fig. 8 and ξ, η, ζ are the Cartesian element coordinates. The general form of $P_q(\xi)$ is given by,

$$P_q(\xi) = \exp(-\alpha\xi)\left[\sum_{n=1}^{3} c_n \exp(-i\beta_n\xi)\right] \quad (q = 1, 2, \ldots, 12). \tag{3}$$

In the above equation, α is the nominal decay coefficient which accounts for the wave damping due to energy dissipation and geometrical divergence of the infinite element. β_n are the nominal R-, S- and P-wave numbers and c_n are the three constants determined by equating the displacement fields of the infinite element and the infinite medium. In the present work, this wave propagation function, $P_q(\xi)$ accounts for the incident wave decay rather than wave reflection after the wave reaches the unit-cell boundary. It is this functionality of the 3D infinite element that enables one to computationally simulate far field regions surrounding the material volume of interest.

In the current work, ABAQUS/explicit was used for performing finite element simulation of the IPC foam unit-cell. As infinite elements are associated with the far field regions, their behavior

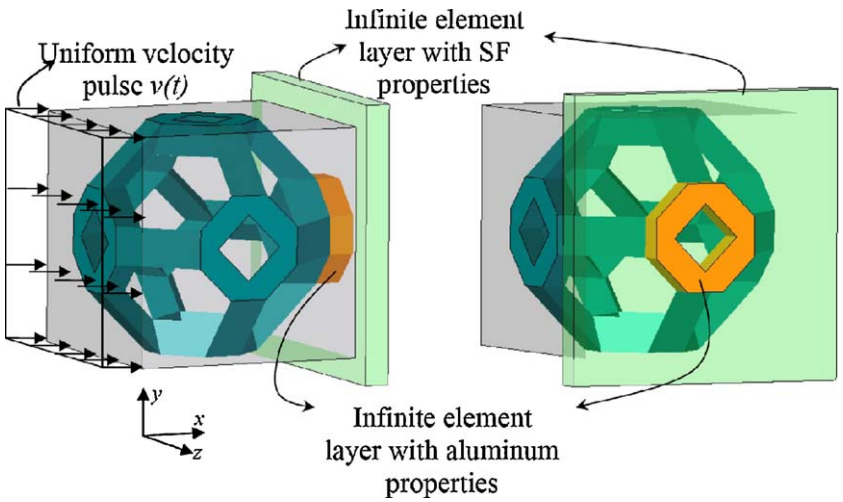

Fig. 9. Schematic of the imposed load and boundary conditions on a IPC foam unit-cell modeled using finite and infinite elements. For clarity infinite element layer is shown on only one face of the unit-cell.

is assumed to be linear and the material response isotropic. The particular infinite element used in this analysis is a 3D, 8 node, one-way infinite brick. Here, "One-way" implies that the infinite elements transmit any stress wave incident on them to a hypothetically infinite distance in one direction and prevent any reflection of stress waves at the boundary of the unit-cell. Further, those infinite elements adjacent to aluminum were assigned the properties of aluminum, and those that are adjacent to SF were assigned the SF properties as seen in Fig. 9. Even though all the sides of the IPC foam have infinite element layers, for the purpose of clarity, the infinite element layer on only one side is shown.

4.4. Boundary conditions

The velocity pulse derived from the measured strain history in the incident bar of the SHPB was imposed for 250 μs on the front face of the unit-cell. Here, the front face of the unit-cell is the boundary between the unit-cell IPC foam and the infinite element layer. The time period of 250 μs was chosen as it is the approximate duration for which the actual test samples were loaded in the SHPB experiments described earlier (Fig. 4).

4.5. Numerical results

The average true stress and average true strain histories of all the elements (aluminum and SF) on the face of the cell directly opposite to the loading face were obtained. From this data, the true stress–strain response of the unit-cell was plotted. The same procedure was followed for all the numerical IPC foam models corresponding to 10%, 20%, 30% and 40% microballoon volume fractions in SF, and the results are shown in Fig. 10 for 20% and 30% cases. Also plotted are the experimental measurements (solid line) obtained from SHPB tests on IPC foams. The agreement between the two is generally good. The minor differences between the experimental results and the simulations are attributed to (a) in the actual specimens micro cracking occurs whereas the numerical model used does not allow any debonding to occur at material interfaces, (b) the material property of aluminum used in the model corresponds to the quasi-static compressive response (this assumption was used considering the fact that aluminum is relatively strain rate independent (Deshpande and Fleck, 2000)) and (c) The infinite elements transmit all the stress waves that are incident on them. In reality, however, there will be stress wave reflections back into the sample at the sample/transmitter bar interface within the duration of 250 μs.

From the finite element analysis, the von-Mises stresses and the equivalent plastic strains were obtained for the unit-cell. From the stress contour plots (Fig. 11), it can be seen that the aluminum ligaments experience the maximum stress, approximately 200 MPa, equal to the yield stress of aluminum. The maximum stress attained by the SF, however, is approximately 70 MPa, which is close to the yield stress of SF-30 obtained from the experiments. From the figures, it is also evident that stress concentrations are present in the vicinity of the ligament intersections. Micrographic inspection of

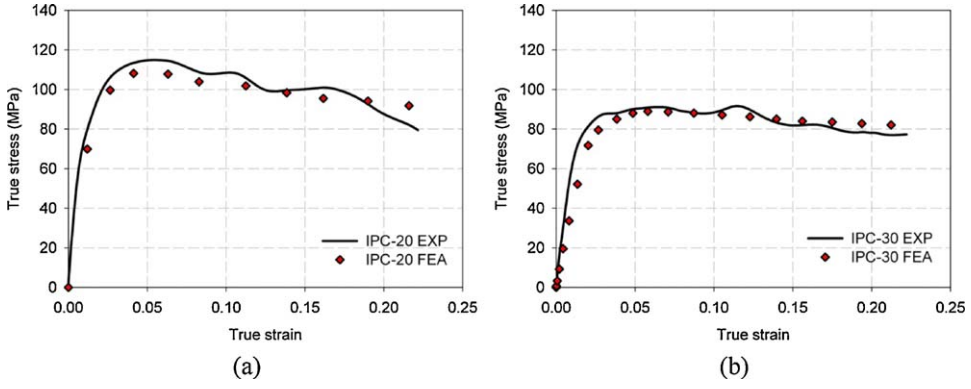

Fig. 10. Comparison of measured stress–strain and dynamic FEA results for two different IPC foams. (a) IPC-20 and (b) IPC-30.

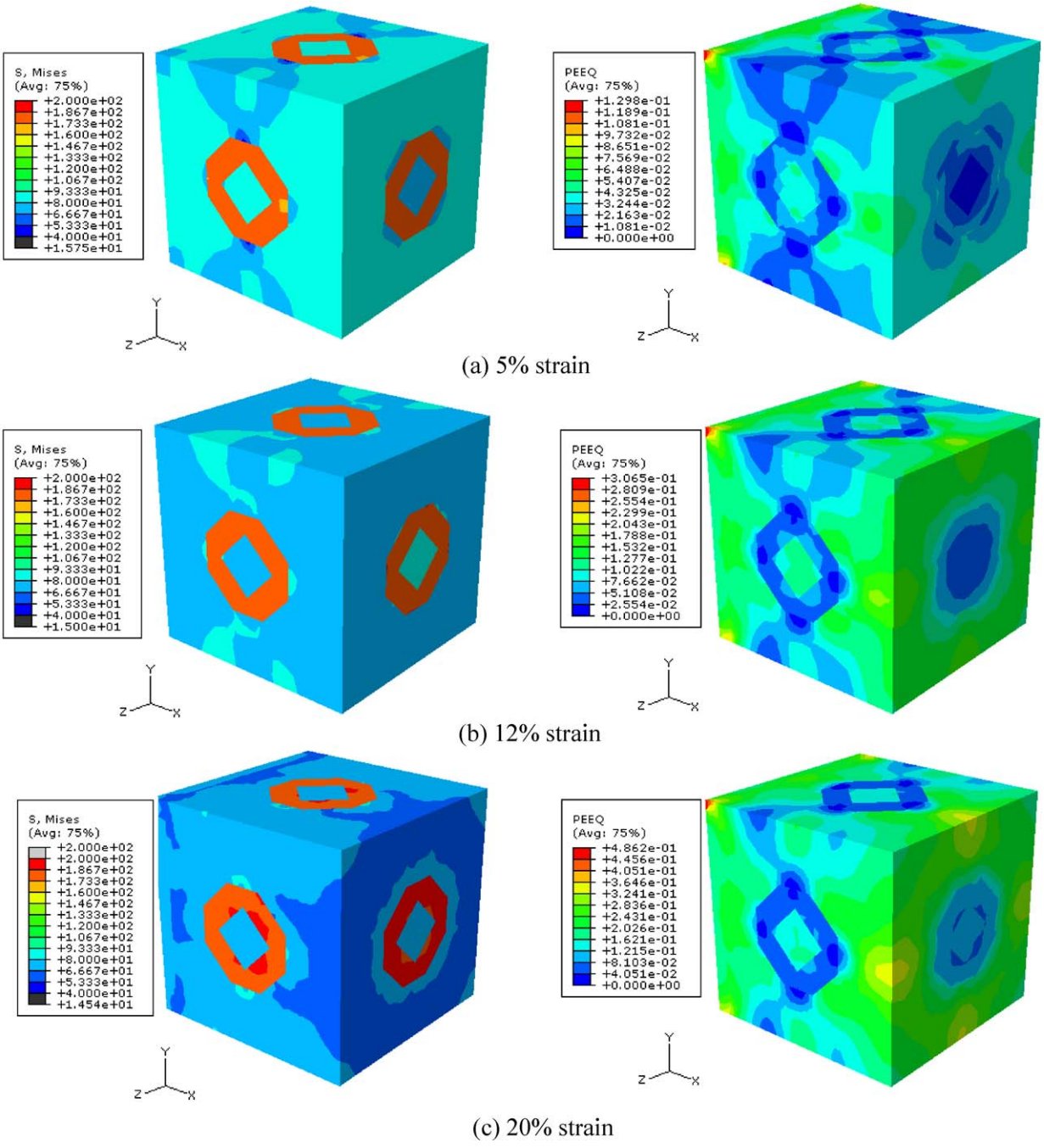

Fig. 11. Contour plots from dynamic FE model for IPC-30. Left side images: von-Mises stress, right side images: equivalent plastic strain (loading is along the *x*-direction).

deformed IPC foam presented by Periasamy et al. (2010) indeed shows debonding between aluminum and SF in the vicinity of a ligament intersection which supports the stress concentration effects observed in the simulation.

The contour plots of the equivalent plastic strain are also shown in Fig. 11. Evidently, the SF region has experienced larger plastic strains compared to aluminum. A more interesting observation from the figures is that the locations of localized maximum plastic strain are not too close to the ligament vertices. This suggests that very close to the vertices, the stiffer aluminum restrains the adjacent SF from deforming as much as the SF regions that are further away.

5. Conclusions

The dynamic compression responses of IPC foams made of SF with 10–40% V_f of hollow glass microballoons were studied at strain rates of ~1500/s. The responses of IPC foams were evaluated relative to their SF counterparts. Micrographs of deformed SF and IPC samples were used to explain the underlying failure mechanisms. A unit-cell based finite element model of an IPC was developed using a Kelvin cell representation of aluminum ligaments of the open-cell scaffold. Experimental stress–strain measurements were used as the material property inputs for the SF region in the finite element IPC model. The aluminum ligaments were assumed to have a

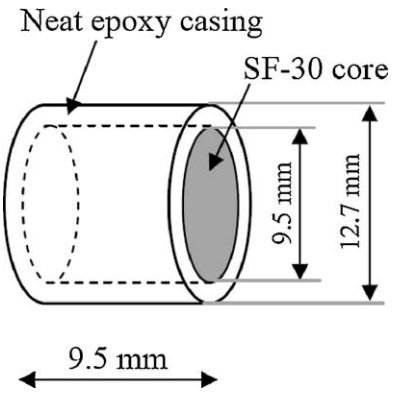

Fig. A1. The bimaterial composite sample geometry used for validating the usage of infinite elements.

bilinear stress–strain behavior with negligible strain rate dependence. Infinite elements were used to model the external surface boundary of the unit-cell to idealize its presence within a large volume of the material. Computational and experimental dynamic compressive stress–strain responses of IPC foam were successfully compared. This numerical model for IPC has the potential to be used as a tool to experiment with new IPCs made of materials other than SF and aluminum. That is, high strain rate performance can be estimated and optimized computationally prior to processing and testing of an IPC.

Acknowledgement

The authors gratefully acknowledge the support of the U.S. Army Research Office through grant W911NF-08-0285.

Appendix A.

First the usage of infinite elements in numerical simulation of the IPC foam was verified. A hypothetical bi-material sample (Fig. A1) was modeled and analyzed for its dynamic compression response using two different finite element based approaches (Fig. A2): (a) using infinite elements and (b) using a long transmitter bar analogous to the long bar in the SHPB experimental set up at one of the sample ends.

The input on the other end in both cases was the measured velocity history obtained from the strain measurements on the incident bar in the SHPB set up used to characterize the IPC foam samples. The hypothetical material model was assumed to be cylindrical with a 9.5 mm diameter SF-30 core and a 1.6 mm thick outer layer of neat epoxy such that the overall diameter was 12.7 mm. The length of the sample was 9.5 mm. The measured stress–strain response of neat epoxy from SHPB experiment at a strain rate of 1200 s^{-1} is shown in Fig. A3(a). The model was discretized using eight node linear hexahedron elements that had a minimum edge length of 0.5 mm. The average stress and strain histories in the (a) sample/infinite element layer and (b) sample/bar interface were obtained for the two cases, respectively. The dynamic stress–strain responses from the two simulations are shown in Fig. A3(b). The two results overlay on top of each other, thus

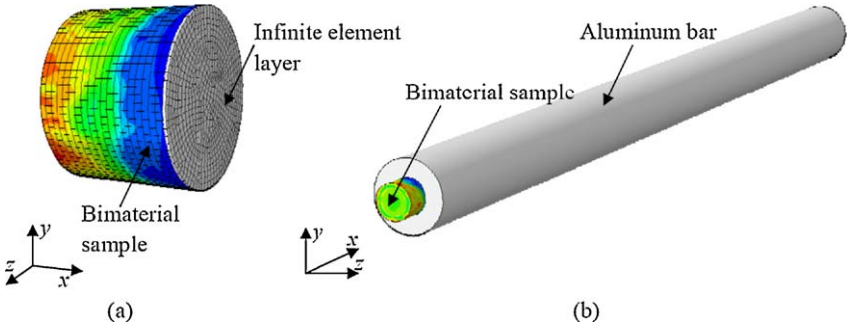

Fig. A2. Finite element model using (a) infinite element layer and (b) long aluminum bar; loading is along the *x*-direction.

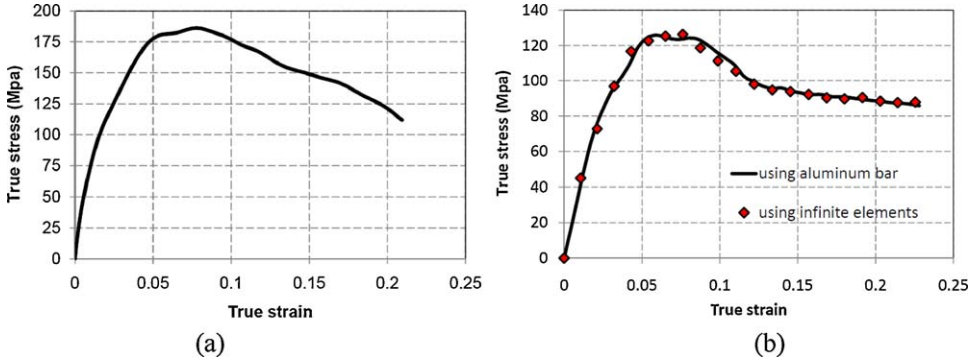

Fig. A3. (a) Dynamic compression response of neat epoxy at a strain rate of 1200 s^{-1}, (b) verification of appropriateness of the implementation of infinite elements by means of simulating a hypothetical bi-material sample.

validating the use of infinite elements for modeling the IPC foam behavior.

References

Bettess, P., 1977. Infinite elements. International Journal for Numerical Methods in Engineering 11 (1), 53–64.

Clarke, D.R., 1992. Interpenetrating phase composites. Journal of the American Ceramic Society 75 (4), 739–759.

Deshpande, V.S., Fleck, N.A., 2000. High strain rate compressive behavior of aluminum alloy foams. International Journal of Impact Engineering 24, 277–298.

Gibson, L.J., 2000. Mechanical behavior of metallic foams. Annual Review of Materials Science 30, 191–227.

Gong, L., Kyriakides, S., Jang, W.Y., 2005. Compressive response of open-cell foams. Part I: Morphology and elastic properties. International Journal of Solids and Structures 42 (5–6), 1355–1379.

Haggblad, B., Nordgren, G., 1987. Modeling nonlinear soil–structure interaction using interface elements, elastic–plastic soil elements and absorbing infinite elements. Computers & Structures 26 (1–2), 307–324.

Malinowski, J.Z., Klepaczko, J.R., 1986. A unified analytic and numerical approach to specimen behavior in the split-Hopkinson pressure bar. International Journal of Mechanical Sciences 28 (6), 381–391.

Mendelson, A., 1983. Plasticity: Theory and Application. Robert E. Krieger Publishing Company.

Meyers, M., 1994. Dynamic Behavior of Materials. John Wiley & Sons, Inc.

Park, W.S., Yun, C.B., Pyun, C.K., 1991. Infinite elements for evaluation of hydrodynamic-forces on offshore structures. Computers & Structures 40 (4), 837–847.

Periasamy, C., Jhaver, R., Tippur, H.V., 2010. Quasi-static and dynamic compression response of a lightweight interpenetrating phase composite foam. Materials Science and Engineering A 527 (12), 2845–2856.

Thomson LXIII, W., 2008. On the division of space with minimum partitional area. Philosophical Magazine Letters 88 (2), A503–A514.

Viladkar, M.N., Godbole, P.N., Noorzaei, J., 1991. Soil structure interaction in plane frames using coupled finite infinite elements. Computers & Structures 39 (5), 535–546.

Zhao, C.B., 2009. Dynamic and Transient Infinite Elements. Springer.

Zhao, C.B., Valliappan, S., 1993. A dynamic infinite element for 3-dimensional infinite-domain wave problems. International Journal for Numerical Methods in Engineering 36 (15), 2567–2580.